Phys. Status Solidi RRL **10**, No. 1, 102–110 (2016) / **DOI** 10.1002/pssr.201510335

Part of Focus Issue on
Carbononics
Eds.: Pawel Hawrylak, Francois Peeters, Klaus Ensslin

pss +++rapid research letters+++
www.pss-rapid.com

Review@RRL

Theory of optical properties of graphene quantum dots

Isil Ozfidan[*,1], A. D. Güçlü[2], Marek Korkusinski[3], and Pawel Hawrylak[1]

[1] Physics Department, University of Ottawa, Ottawa, Canada K1N 6N5
[2] Department of Physics, Izmir Institute of Technology, IZTECH, 35430, Izmir, Turkey
[3] National Research Council of Canada, Ottawa, Canada K1A OR6

Received 9 September 2015, revised 18 October 2015, accepted 19 October 2015
Published online 26 October 2015

Keywords graphene quantum dots, optical spectra, mean field, configuration interaction

[*] Corresponding author: e-mail aozfi017@uottawa.ca

We present here a theory of the optical properties of graphene quantum dots (GQDs) with tunable band gaps by lateral size confinement, from UV to THz. Starting from the Hartree–Fock ground state, we construct the correlated many-body ground and excited states of GQDs as a linear combination of a finite number of electron–hole pair excitations. We discuss the evolution of the band gap with size and its renormalization by self-energy and excitonic effects. We calculate and analyze the dipole moments of graphene quantum dots that possess a degenerate valence and conduction band edge, and construct a characteristic exciton and biexciton spectrum. We find an exciton band consisting of a pair of robust, spin singlet bright exciton states and a band of dark, spin singlet and spin triplet, exciton states at lower energies. We predict a characteristic band of biexciton levels at the band edge, discuss the Auger processes and identify a biexciton–exciton cascade. Our theoretical results are compared with experimental linear absorption and non-linear transient absorption spectra of colloidal GQDs. We next discuss the optical properties of triangular GQDs with zigzag edges whose magnetic moment can be controlled by gates. The control over the magnetic moment through carrier density manipulation results in optical spin blockade and gate tunable optical properties over a wide range of photon energies.

1 Introduction The ability to open up a gap in bulk graphene, a semimetal, by changing the size, shape, edge character, number of layers, carrier density and screening by the substrate offers an exciting possibility of simultaneously tuning the electronic [1–10], magnetic [5, 9–17] and, most importantly, optical properties of graphene quantum dots (GQD) [18–30] continuously from THz to UV. In this contribution, we discuss the effects of electron–electron interactions on the energy gap and optical properties of graphene quantum dots.

The dependence of the energy gap on the number of atoms N, the size and the shape of the graphene quantum dots has already been introduced in this issue by Ozfidan et al. The optical gap determines the lowest energy photon that can be absorbed. For hexagonal quantum dots with armchair edges, the tight binding gap decreases as the inverse of the square root of N, as expected for confined Dirac fermions with photon-like linear energy dispersion ($E_{\rm gap} \propto k_{\rm min} \approx 2\pi/\Delta x \propto 1/\sqrt{N}$). Similarly, the valence band (VB)-conduction band (CB) energy gap in the triangular, zigzag edged structures also follows the Dirac fermion power law, $E_{\rm gap} \propto 1/\sqrt{N}$, allowing for the variation of the energy gap from ≈2.5 eV (green light) for a quantum dot with ≈100 atoms to ≈30 meV (8 THz) for a quantum dot with a million atoms and a diameter of ≈100 nm. In addition to these transitions, in triangular GQDs with zigzag edges, the energy spectrum contains a shell of degenerate levels at the Fermi level. The presence of the degenerate, zero-energy states in the middle of the energy gap results in additional transitions with energies lower than that of the VB–CB transitions which are needed for e.g., intermediate band solar cells. Moreover, the presence of the spin polarized band of partially occupied degenerate states at

the Fermi level provides the unique opportunity to simultaneously control magnetic and optical properties of TGQDs [24]. This offers interesting opportunities in opto-electronic, opto-spintronic and intermediate-band solar cell photo-voltaic applications. GQDs may also be exploited in quantum communication, e.g., in the generation of entangled photon pairs [27]. A detailed analysis of the zigzag edges on the magnetic properties of triangular GQDs were discussed in this issue by Güçlü et al.

2 Interaction of light with graphene quantum dots Light-matter interactions are introduced at a single particle level. In Coulomb gauge, interaction of an electron with the electromagnetic field given by weak vector potential $\boldsymbol{A}(\boldsymbol{r},t)$ is written as

$$H_{\text{int}} = \frac{e}{m}\boldsymbol{A}(\boldsymbol{r},t)\cdot\boldsymbol{p}\,, \tag{1}$$

where $\boldsymbol{p}$ is the momentum of the electron. The electromagnetic field is described by the vector potential $\boldsymbol{A}(\boldsymbol{r},t) = A_0\hat{\varepsilon}\left[e^{i\boldsymbol{k}\cdot\boldsymbol{r}-i\omega t} + e^{-i\boldsymbol{k}\cdot\boldsymbol{r}+i\omega t}\right]$, where $\hat{\varepsilon}$ is the polarization of light.

The absorption/emission spectrum of a quantum dot is obtained from Fermi's golden rule:

$$A(\omega) = \sum_{q,p} W_q |\langle p|\, H_{\text{int}}\, |q\rangle|^2\ \delta(E_p - E_q \pm \omega)\,, \tag{2}$$

where E_p, E_q are the energies of the initial and the final quantum dot electronic states $|q\rangle = \sum_i k_{q,i}\,|\varphi_i\rangle$ participating in the excitation process, W_q is the occupation probability of the initial state and ω is the energy of the photon with –(+) sign corresponding to absorption (emission).

Assuming the wavelength of the light absorbed during the transition is much greater than the size of the graphene quantum dot, $e^{i\boldsymbol{k}\cdot\boldsymbol{r}} \simeq 1$, and the matrix elements of the light matter interaction Hamiltonian can be expressed in terms of the dipole elements,

$$\langle p|\, H_{\text{int}}\, |q\rangle = i(\omega_{pq})\ A_0\hat{\varepsilon}\cdot\langle p|\, e\hat{r}\, |q\rangle\,, \tag{3}$$

where $\langle p|\, e\hat{r}\, |q\rangle = d(p,q)$ is the dipole element between states p and q, evaluated in the basis of atomic p_z orbitals $\varphi(\boldsymbol{r}-\boldsymbol{R}_i)$:

$$\langle p|\,\boldsymbol{r}\,|q\rangle = \sum_{i,f} k^*_{p,f}k_{q,i}\int \mathrm{d}\boldsymbol{r}\ \varphi^*(\boldsymbol{r}-\boldsymbol{R}_f)\,\boldsymbol{r}\varphi(\boldsymbol{r}-\boldsymbol{R}_i)\,. \tag{4}$$

Replacing $\boldsymbol{r}\to\boldsymbol{r}+\boldsymbol{R}_f$ and taking into account only the nearest neighbor (NN) $\langle i,f\rangle$ and the next nearest neighbor (NNN) $\langle\langle i,f\rangle\rangle$ terms, the dipole element is rewritten as [18],

$$\langle f|\,\boldsymbol{r}\,|i\rangle = D(\hat{R}_i - \hat{R}_f)\,\delta_{\langle fi\rangle} + d(\hat{R}_i - \hat{R}_f)\,\delta_{\langle\langle fi\rangle\rangle} + \hat{R}_l\delta_{lj}\,, \tag{5}$$

where the coefficients $D = \int \mathrm{d}\boldsymbol{r}\ \varphi_z^*(\boldsymbol{r})\,\boldsymbol{r}\varphi_z(\boldsymbol{r}-\boldsymbol{R}_{\langle fi\rangle})$ = 0.343542 a.u. and $d = \int \mathrm{d}\boldsymbol{r}\ \varphi_z^*(\boldsymbol{r})\,\boldsymbol{r}\varphi_z(\boldsymbol{r}-\boldsymbol{R}_{\langle\langle fi\rangle\rangle})$ = 0.0873 a.u. are computed using the Slater-type p_z orbitals for NN and NNN orbitals respectively and $\hat{R}_i$ are unit vectors. In calculation of the dipole elements, contributions from the overlap of the non-orthogonal Slater-type orbitals are neglected.

One can write the light-matter interaction in terms of the polarization operator $\hat{P}^+$ and photon creation/annihilation operators $a^+(a^-)$ as $H_{\text{int}} = \hat{P}^+a^- + \hat{P}^-a^+$. In second quantization, suitable for many-electron quantum dots, the polarization operator $\hat{P}^+ = \sum_{pq\sigma} d(p,q)\,b^+_{p\sigma}b_{q\sigma}$, creates a single pair excitation by moving an electron from a state q to state p while annihilating a photon. Here $b^+_{p\sigma}(b_{q\sigma})$ creates (annihilates) an electron in a state $p\sigma$.

As described in detail in Ref. [26], for 3-fold symmetric GQDs such as benzene, hexagonal and triangular GQDs, the eigenstates can be characterized according to their angular momenta projections, m, and the dipole elements can be simplified to reveal the selection rules for angular momenta projections of the eigenstates. In order to distinguish states according to m, the GQDs are divided into three segments by defining 3 symmetry axes. Introducing a rotation operator, $\hat{R}$, that maps rotationally equivalent atoms from each segment onto one another with a phase of $e^{im2\pi/3}$, where $m = 0, 1, 2$, vectors invariant under this rotation are obtained. Note that $m = 2$ is equivalent to $m = -1$ and we will often implicitly use this relation. Once the Hamiltonian is separated into three angular momentum blocks, each block is diagonalized to obtain angular momentum separated single particle eigenvectors and energies with eigenvalue index ν and quantum number m, $|\nu, m\rangle$. The eigenvalues $m = 1$, $m = 2$ (or $m = \mp 1$) are degenerate as their corresponding eigenvectors are complex conjugates of one another.

Expanding the rotationally invariant eigenvectors $|\nu, m\rangle$ in terms of localized orbitals and assuming circular polarization of light $\varepsilon_\pm$, following selection rule for the dipole element between the eigenstates $|\nu, m\rangle$ can be derived [26],

$$\langle \nu', m'|\,\boldsymbol{\varepsilon}\cdot\boldsymbol{r}\,|\nu, m\rangle = \delta_{m',m\pm1}C_{m,m',\nu,\nu'}\,, \tag{6}$$

where C is a constant determined numerically.

3 Many body Hamiltonian and ground and excited states In a charge neutral graphene quantum dot with one electron per orbital, there are many ways of placing N electrons on N orbitals. The ground state of N non-interacting electrons can be written as a single Slater determinant, created by placing N electrons on the lowest N single-particle orbitals. Turning on the interactions, there will be a competition between minimizing the kinetic energy versus minimizing the interactions between electrons. In order to find an approximate ground state of an interacting electron system that can be expressed as a single Slater determinant, the Hartree–Fock (HF) theory can be used as described by Ozfidan et al. in this issue.

In general, the wavefunction of an interacting system cannot be expressed as a single Slater determinant. This is due to the correlations among electrons that cannot be described with a mean-field approach. In order to account for these correlations we need a linear combination of many body configurations. Starting with the HF ground state that is obtained by placing the electrons in the lowest HF-quasiparticle levels, electron–hole pairs are generated by moving an electron from the valence band to the conduction band, leaving a hole behind. In the configuration interaction (CI) method, a Hamiltonian that is generated in the basis of HF ground state and electron hole pairs is diagonalized to obtain the exact ground state of the correlated system. The new correlated ground state can be expressed as a linear combination of Slater determinants. For small structures with several electrons, an exact ground state can be obtained by creating all possible excitations out of the HF ground state. However the number of configurations grows factorially with the number of states and electrons in hand, making the configuration interaction method very computationally expensive. Thus, the CI-space is truncated to obtain a good approximation to the correlated ground state.

Since the starting point is the HF ground state, it is beneficial to express the Hamiltonian in terms of the HF operators $b^{+}_{p\sigma}(b_{p\sigma})$ that creates (annihilates) an electron on HF quasiparticle level q. As introduced in Ozfidan et al. in this issue, the configuration interaction Hamiltonian has the following form,

$$H = \sum_{p,\sigma}^{N} \varepsilon_{p\sigma} b^{+}_{p\sigma} b_{p\sigma} + \frac{1}{2} \sum_{p,q,r,s,\sigma,\sigma'}^{N} \langle pq|\, V_{\mathrm{HF}}\, |rs\rangle\, b^{+}_{p\sigma} b^{+}_{q\sigma'} b_{r\sigma'} b_{s\sigma} - \sum_{p,q,\sigma}^{N} V^{\mathrm{MF}}_{pq\sigma} b^{+}_{p\sigma} b_{q\sigma}\,, \tag{7}$$

where $V^{\mathrm{MF}}_{pq\sigma}$ is the mean-field interaction among quasi electrons.

In this paper, because we are interested in excitons (X) and bi-excitons (XX), we limit the CI subspace to include up to two quasi electrons and quasi holes. Upon diagonalization, the correlated X and XX states are expressed as a linear combination of electron–hole pairs generated out the HF ground state.

4 Excitons in hexagonal and triangular quantum dots In order to calculate the absorption spectrum, in addition to the dipole matrix elements, one needs the correlated ground and excited states. In calculating the ground state via the HF method, it is assumed that the valence band is filled with electrons up to the Fermi level. Then placing an electron on any one of the HF levels, it already feels the presence of a filled valence band as the HF eigenenergies include *self energy* that represents the mean field interaction of an electron with the filled valence band. For a graphene quantum dot with a band gap, the *self energy*, $\Sigma(p)$, of an electron placed on HF level p is expressed as

$$\Sigma(p) = \sum_{q=0}^{N_{\mathrm{Fermi}}} \left(2\langle pq|\, V\, |qp\rangle - \langle pq|\, V\, |pq\rangle\right), \tag{8}$$

where the summation is over all filled levels q. Using this definition of self energy, the ground state E_{GS} energy can be expressed as

$$E_{\mathrm{GS}} = \sum_{p=0}^{N_{\mathrm{Fermi}}} \left(2\varepsilon_p - \Sigma(p)\right), \tag{9}$$

where ε_p is the eigenenergy of the HF level p. The 2 in front of ε_p accounts for up and down spins occupying each valence orbital. Since energy of each HF orbital already includes self energies, one would be over counting the interactions just by adding up the eigenvalues of the HF levels. To avoid the over counting, a self energy per orbital is subtracted in the equation above.

Moving an electron from a valence state (i,σ) with $i \le N/2$ to a conduction band state (j,σ) with $j > N/2$, single pair excitations are created. Taking the symmetric and antisymmetric combinations of single pair excitations with opposite spins, the singlet and triplet configurations are obtained as

$$|j,i,S/T\rangle = \frac{(b^{+}_{j\uparrow} b_{i\uparrow} \pm b^{+}_{j\downarrow} b_{i\downarrow})}{\sqrt{2}} |\mathrm{GS}\rangle\,, \tag{10}$$

where + and – signs correspond to a singlet and a triplet, respectively. Following the definition of self energy, energies of these excitations measured from ground state energy E_{GS}, are obtained as

$$E(j,i)_{S/T} = \varepsilon_j - \varepsilon_i - \langle ji|\, V\, |ij\rangle + \langle ji|\, V\, |ji\rangle \pm \langle ji|\, V\, |ji\rangle\,. \tag{11}$$

In the expression above, the third term $-\langle ji|\, V\, |ij\rangle$ is the attraction between the electron and the hole and the fourth term, $+\langle ji|\, V\, |ji\rangle$, is the short ranged, repulsive exchange interaction. Note that in vertex corrections, thedirect Coulomb interaction is attractive while exchange is repulsive; opposite of the contributions to quasiparticle energies and consistent with Ward identities. The singlet and triplet states of electron–hole pair are distinguished by the last term, $\pm\langle ji|\, V\, |ji\rangle$, which ensures that triplet is the lowest energy state and the singlet/triplet splitting is given by $2\langle ji|\, V\, |ji\rangle$, twice the exchange interaction. The pair excitations (j,i) are not eigenstates of the interacting system, they are mixed by Coulomb interactions resulting in correlations between excitations.

We will now study the role of each interaction term by turning them on, one by one, in GQDs with degenerate valence and conduction band edges, as depicted in Fig. 1.

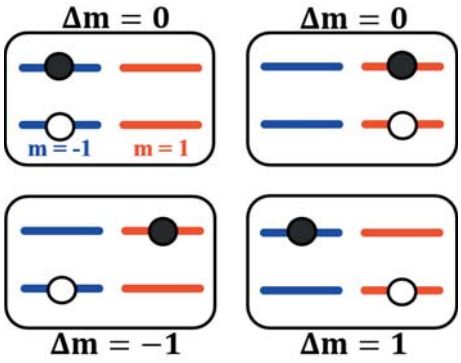

Figure 1 Band edge exciton configurations. Blue and red corresponds to $m = -1$ and $m = 1$ levels. The excitons are separated according to change in angular momentum $\Delta m = m_{\text{electron}} - m_{\text{hole}}$.

The 8×8 electron–hole pair subspace created at the degenerate band edge can be block diagonalized according to Δm. Since the degenerate levels have $m = \pm 1$, removing an electron from the valence band level with $m = -1$ and placing it on the conduction band level with $m = -1$ will create a $\Delta_m = 0$ configuration. However, if the removed electron is placed on the $m = 1$ conduction band level, the electron–hole pair would have $\Delta m = +2$ or, equivalently, $\Delta m = -1$. These configurations are depicted in Fig. 1.

Since there are two electrons on each level, a spin up and a spin down, the $\Delta m = 0$ subspace contains 4 pairs while the $\Delta m = \pm 1$ subspaces each have 2 pairs at the band edge. Within each subspace linear combinations of these configurations result in the singlet and triplet states, further reducing the size of each subspace (Fig. 2). For example, the $\Delta m = 1$ configuration for spin up and spin down electrons can be combined to give the non-interacting singlet and triplet states.

Now, as an example, let us turn on different interactions one by one and examine their effects on the level ordering for a 168 atom 3-fold symmetric GQD obtained using colloidal chemistry [19, 26, 27, 31]. Singlet or triplet, each pair will have the direct electron–hole interaction correction to its energy. The far left and right columns in Fig. 2 depict the energies of $\Delta m = 0$ and $\Delta m = \pm 1$ pairs after the inclusion of self energies and direct interaction corrections. Turning on the exchange interaction separates the singlets and triplets as depicted in the second columns from right and left in Fig. 2. The $\Delta m = \pm 1$ states do not change any further since each total-spin subspace contains only one state. Within $\Delta m = 0$, each total spin subspace has 2 interacting states. Correlations among these states cause them to separate in energy. Since in a triplet the attractive scattering is not partially compensated by repulsive exchange interaction and is stronger, the repulsion of triplet levels is greater than singlet levels, as shown in the center column of Fig. 2.

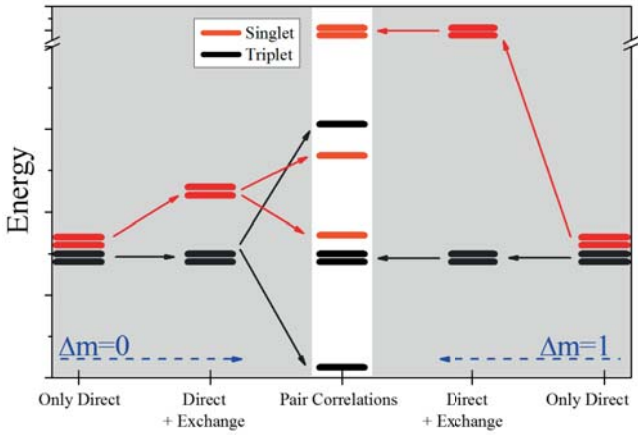

Figure 2 Evolution of the lowest 8 excitations with inclusion of different interaction terms [26].

As a result, at the band edge, there are two bright degenerate singlet exciton states and at lower energies a band of dark excitons composed of two orbitally dark singlets and four dark triplets, as shown in the center column of Fig. 2.

Figure 3 shows the evolution of the band edge excitonic spectrum associated with the degenerate band edge states of a GQD calculated in different levels of approximations. Figure 3(a) shows the absorption spectrum of the non-interacting triangular GQDs with $N = 168$ in the tb approximation. At this level, the energy of the absorption peak is equivalent to the single particle tb band gap. Figure 3(b) shows the absorption in the tb + HF approximation. We see that energy blue-shifts due to inclusion of self energies of the electron and the hole. Figure 3(c) shows the band-edge exciton spectrum calculated using the configuration interaction method. Inclusion of spin and electron–hole interactions (vertex corrections) red-shifts the absorption spectrum. Most importantly, we see the structure of the band edge excitonic spectrum where a band of dark

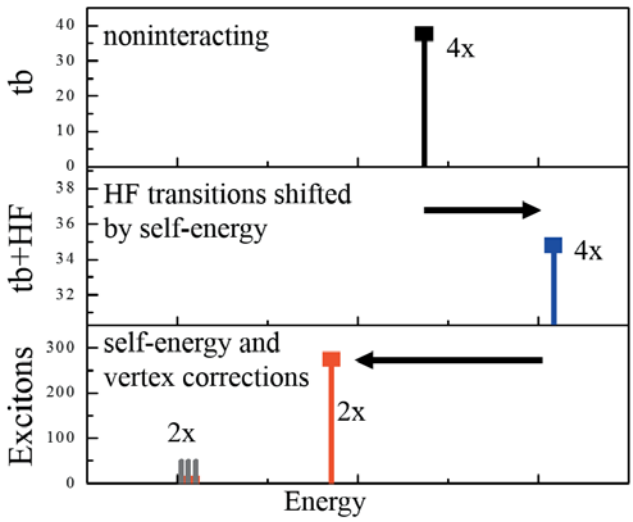

Figure 3 Evolution of the band edge absorption peak with increasing accuracy of approximation (a) Tight binding, (b) Hartree Fock, (c) configuration interaction [26].

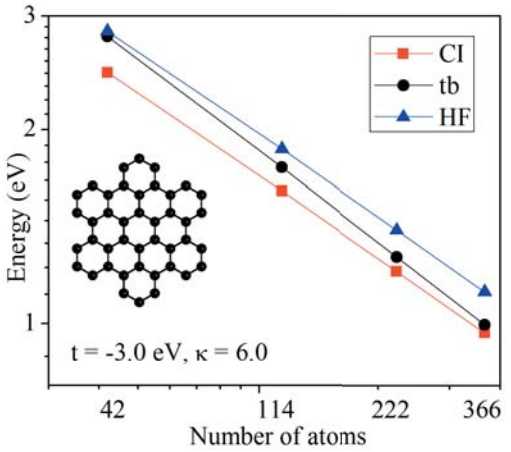

Figure 4 Evolution of the energy of the bright band edge excitons with size of hexagonal graphene quantum dots with armchair edges. For comparison, the plot also depicts the tight binding and the Hartree–Fock gaps.

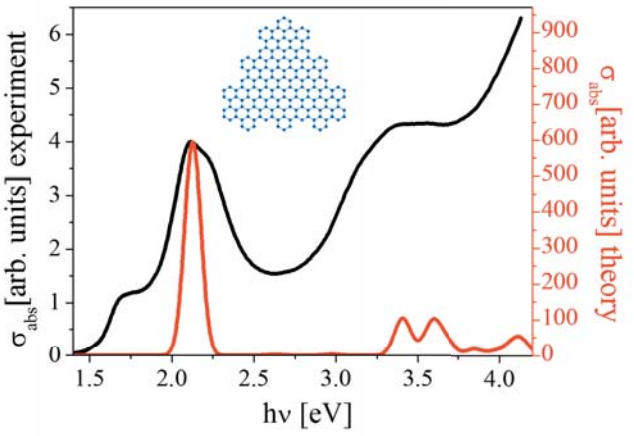

Figure 5 Absorption spectrum of a 168 atom colloidal graphene quantum dot fitted to the experiment. $\kappa = 5.0$, $t = -4.2$ eV, $t' = -0.1$ eV. Higher order corrections due to XX's are included in the calculation of the spectrum

singlet and triplet exciton states appears at lower energy separated from the two bright, degenerate, singlet exciton states. The structure of the exciton band and presence of the degenerate bright singlet excitons are robust and are independent of the shape as long as the 3-fold rotational symmetry is preserved. For the quantitative absorption spectrum of the band edge, additional HF levels higher/lower in energy must be included. Furthermore, although two-pair excitations do not directly appear in the linear absorption spectrum, their inclusion modifies the energies of the single pair excitons.

We now turn to the size dependence of the bright exciton spectrum. Figure 4 depicts how the energy of the bright degenerate exciton peak calculated in the tb + HF + singleX-CI approximation evolves with the size N of the hexagonal quantum dot. For comparison, the tight binding and the Hartree–Fock gaps are also shown. All calculations assume identical screening of Coulomb interactions by environment, with $\kappa = 6$. We see that for small GQD ($N = 42$) HF blue shift is small and the only renormalization is the electron–hole attraction. For largest GQD we find the HF renormalization large but compensated by the vertex correction so the tight binding and the bright excitonic transitions are very close in energy.

Even though we see both the blue and the red-shifts, the tight binding appears to provide a good method in predicting the relation between the size and the energy of the bright, band edge peak. For additional discussion of the renormalization of the absorption by e–e interactions we refer the reader to Ref. [29].

5 Absorption spectrum of colloidal graphene quantum dots Figure 5 compares the experimental [19] and calculated absorption spectra for a 3-fold symmetric, 168 atom colloidal graphene quantum dot. The screening constant, $\kappa = 5.0$ and tunnelling matrix elements $t = -4.2$ eV are set to match the position of the main peak and the reduced absorption observed right after the main peak in the experimental spectrum. The main peak at $E = 2.1$ eV is associated with the doubly degenerate, orbitally bright singlets at the band edge. The absorption threshold at $E = 1.6$ eV is attributed to the calculated orbitally dark singlets. Coupling to phonons, impurities or breaking of the symmetry due to, e.g., charge and spin fluctuations in the surrounding fluid, can lead to optical activation of these levels [26, 31–33]. Assuming that this peak is indeed due to the orbitally dark singlets and spin dark triplets, the theory leads to a significantly underestimated bright singlet dark triplet splitting when compared with experiments. The main reason for such discrepancy may be the uniform treatment of screening, independent of the length scale.

6 Biexcitons and higher order excitations Double excitations are created by moving two electrons from the valence band to the conduction band, leaving two holes behind; $|p\sigma_1, m\sigma_2; q\sigma_1, n\sigma_2\rangle = b^+_{p\sigma_1} b^+_{m\sigma_2} b_{q\sigma_1} b_{n\sigma_2} |HF_{GS}\rangle$. At the band edge one can create 18 double excitations. Out of these, ten have $S = 0$. Just as for single pair excitations, due to electron–hole pair correlations all biexciton configurations will be mixed with one another.

The $S = 0$ band edge exciton and biexciton levels are depicted in Fig. 6. The biexciton levels are color coded according to the most probable two-pair configuration and its excitonic constituents. For example, the biexciton level XX_{10} is composed of a $\Delta m = 1$ and a $\Delta m = 0$ exciton which are assigned by the colors red and blue, respectively, giving the XX_{10} the blue−red color.

The energy of a biexciton, based on the most probable two-pair configuration is calculated as $E_{XX} = E_{X_1} + E_{X_2} + \Delta_{XX}$ where E_{X_i} are the energies of the excitons forming the biexciton and Δ_{XX} is the biexciton binding energy. The sign of Δ_{XX} can be positive or negative, corresponding to excitons attracting (binding) or repelling (unbinding) each other, respectively. It is also an

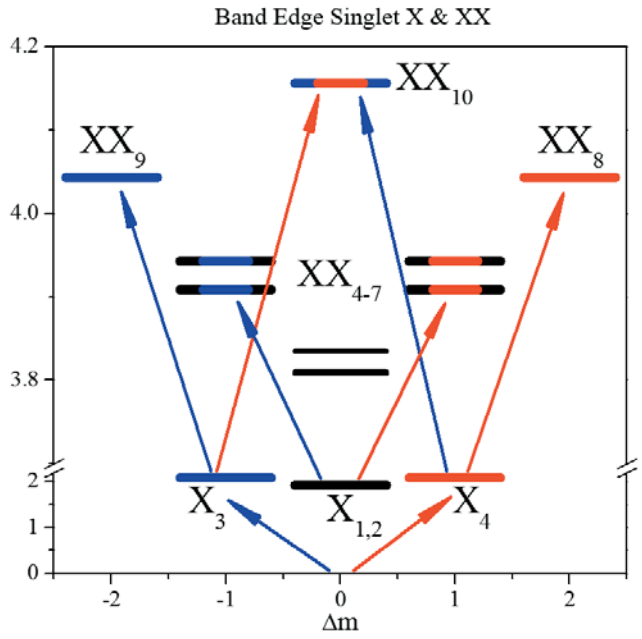

Figure 6 Band edge $S = 0$, exciton and biexciton levels. Levels are color coded according to their exciton content. Blue and red correspond to $\Delta m = -1$ and $\Delta m = 1$ excitons while $\Delta m = 0$ is shown in black. The blue and red arrows depict the allowed transitions via circularly polarized light.

indicator of degree of correlation, which is measured by the number of two-electron–hole configurations contributing to the XX state.

Experimentally, the binding energy can be obtained in transient absorption experiments and can be compared with theoretical calculations. Although the two lowest-energy singlet states ($LX = X_{1,2}$) are not accessible directly from the ground state, they are accessible in transient absorption experiments [26, 31, 32]. Theoretical calculations suggest that the only optically accessible biexciton levels from LX are XX_{4-7}. Starting with either one of the LX levels, optically adding $X_{3,4}$ will generate these levels. Then the biexciton binding energies are calculated as $\Delta_{XX(4,7)} = E_{XX(4,7)} - E_{LX} - E_{X(3,4)} = 104 - 145$ meV. Comparing the predicted transient absorption spectra with the experimentally measured one, the source of the absorption peaks in the experiment can be determined and the binding energies can be fitted. The experimental prediction for the binding energies of $\Delta_{XX(4-7)} = 0.17 \pm 0.01$ eV are in good agreement with the theory [28, 31].

7 Biexciton–exciton cascade The process of XX-X cascade proposed for the generation of entangled photon pairs in semiconductor quantum dots [34–37] relies on two degenerate exciton levels. The degeneracy is a result of strong spin–orbit interaction. Unlike semiconductor quantum dots, graphene has a weak spin–orbit coupling [1–4, 6–18, 20, 24, 38–43] yet we have shown the presence of degenerate bright exciton states. Hence GQDs could potentially replace semiconductor QDs in entangled photon generation if a well defined biexciton level could be identified [27].

Since the excitons that contribute to a XX–X cascade need to be optically active, only the degenerate X_3 and X_4 can participate in entangled photon generation. Due to optical selection rules, there are only two ways of accessing these degenerate states from a biexciton; emitting a photon with σ^- or σ^+ polarization. Then the only possible biexciton states that would emit to these excitons are obtained by creating an electron hole pair with $\Delta m = 1$ on a $(m = 1) - (m = 2)$ valence–conduction pair or with $\Delta m = -1$ on a $(m = 2) - (m = 1)$ pair. At the band edge, there are only three states that fit into this description; two of which are degenerate $XX_{8,9}$, while the third one is the highest energy band edge biexciton XX_{10}.

From a superposition of degenerate biexcitons $XX_{8,9}$, the emerging photons will be polarization entangled. However if the initial state is either one of them, then the polarization of the photons emerging will collapse to a certain handedness, destroying the entanglement.

Preparing the initial state as XX_{10}, the entangled Bell-state of the two photons generated in its radiative recombination will be polarization entangled:

$$|\psi\rangle = \frac{1}{\sqrt{2}}\left(|\sigma^-\sigma^+\rangle + |\sigma^-\sigma^+\rangle\right). \tag{12}$$

8 Auger processes As more and more electron–hole pairs are included, the CI subspace grows factorially. Since the CI Hamiltonian is a two-body interaction Hamiltonian, N-pair excitations within a ±2-pair range interact with one another directly. For example, a 3-pair exciton will have first order contributions from a range of 1-pair to 5-pair excitations only. Beyond that, all other N-pair excitations have second or higher order contribution to the energy of a 3-pair exciton. As a result, in a weakly interacting quantum dot, exciton and biexciton energies will not be greatly affected by the presence of excitations beyond 4-pair.

For strongly interacting electrons however, interactions can no longer be considered as perturbations. Thus, excitations interact with one another strongly and higher order excitations become important in determining the true ground state.

Due to the higher number of quasi particles, there are more pair-interaction terms one would need to consider. Furthermore, due to correlations among electron–hole pairs, even if a pure-biexciton configuration is the most probable configuration in a state, there can be significant contributions from excitons and other biexcitons with similar energies. The XX spectral function can help assess the *purity* of biexcitons and understand Auger processes.

In quantum dots, Auger recombination is important in determining biexciton lifetime. It is a non-radiative process in which a biexciton is converted into an excited exciton. Starting with a biexciton, one of the electron–hole pairs can recombine and give the excess energy to the remaining

electron (hole), exciting it to a higher (lower) conduction (valence) band, creating excited excitons. This process may decrease the lifetime of the biexciton, making it short-lived and difficult to detect.

In order to properly capture all Auger processes, the CI subspace must include the excited exciton levels that can be generated through non-radiative recombination of a pair in a biexciton. Concentrating on the band edge biexcitons, CI subspace should include all single pair excitations that can be generated in a 3× band gap energy window of HF states [27].

Calculation of the spectral function requires, separately, the eigenstates and eigenvalues of the *mixed* system (GS + X + XX) and the eigenstates and values of the *conserved* system in which only two electron–hole pair configurations are taken into account. Finally, both bases need to be restricted in the same manner; by including all X's and XX's within the window of $3\times E_g$ to capture Auger processes at the band edge, which results in a subspace of 2×10^5 configurations. After exact diagonalization of the Hamiltonians their eigenfunctions are obtained as

$$|\Phi_\nu\rangle = k_0^\nu\,|\mathrm{GS_{HF}}\rangle + \sum_{mn\sigma} k_{mn}^{\nu(1)}\,|i\sigma;j\sigma\rangle + \sum_{pmqn}\sum_{\sigma_1\sigma_2} k_{pmqn}^{\nu(2)}\,|p\sigma_1,m\sigma_2;q\sigma_1,n\sigma_2\rangle + \ldots \quad (13)$$

for the mixed system corresponding to eigenvalues E_ν and [44]

$$|\mathrm{XX}\rangle_\eta = \sum_{pmqn}\sum_{\sigma_1\sigma_2} k_{pmqn}^{\eta}\,|p\sigma_1,m\sigma_2;q\sigma_1,n\sigma_2\rangle\,. \quad (14)$$

for the conserved system with eigenvalues E_η. In order to quantify the degree of mixing between a biexciton state $|\mathrm{XX}\rangle_\nu$ and the rest of the excitations, the spectral function $A_{\eta,\mathrm{XX}}(\nu)$, is introduced as

$$A_\eta(E) = \sum_\nu |_\eta\langle \mathrm{XX}\,|\,\Phi_\nu\rangle|^2\,\delta(E_\nu - E)\,,$$

$$= \sum_\nu \left|\sum_{pmqn}\sum_{\sigma_1\sigma_2}\left(k_{pmqn}^{\eta}\right)^{*} k_{pmqn}^{\nu(2)}\right|^2 \delta_{E_\nu - E}\,. \quad (15)$$

This function projects a conserved biexciton state, XX_η, onto the states of the mixed system [44]. It approaches $A_\eta(E_\nu)\to 1$ for a weakly coupled system where E_ν corresponds to the eigenstate mainly composed of XX_η in the mixed system. As an example, the spectral function of the XX_{10} state ($\eta = 10$) of the conserved system is shown in Fig. 7. The highest $A_{10}(E_\nu)$ peak with a value of 0.90 corresponds to the energy of XX_{10} in the mixed state. The size of this peak tells us that XX_{10} is coupled weakly to the excited excitons in the mixed system and is expected to be stable against Auger recombination [27].

9 Optical spin blockade in triangular quantum dots with zigzag edges In triangular graphene quantum dots (TGQD) with zigzag edges, the existence of the zero energy band allows for the control of magnetic and optical properties of GQDs [18, 42, 45]. As depicted in the optical joint density of states for a 97 atom TGQD with zigzag edges in Fig. 8, in addition to the valence-conduction transition (VC), there are intermediate energy optical transitions allowed through valence-to-zero (VZ) and zero-to-conduction (ZC) transitions in the TeraHertz energy spectrum within the zero energy band (ZZ) that do not exist for sublattice symmetry preserved GQDs. The energies of ZZ transitions are determined by next nearest neighbour hopping and electron–electron interactions as without the two the levels are degenerate.

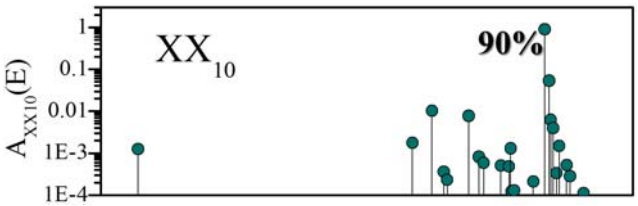

Figure 7 Spectral function of the highest energy band edge biexciton.

At half filling, due to exchange interaction, the electron spins of the zero energy band align. As a result, with a single electron per level, transitions to and from the zero-energy band are allowed. However, the ZZ transitions are not allowed as a photon cannot flip the spin of an electron.

The carrier density, thus, the filling of the zero energy shell, can be tuned by external metallic gates or doping. The addition or removal of an electron to the spin-polarized band of electrons greatly influences the optical transitions. Increasing the shell filling, the number of available states at the zero energy band reduces, quenching the VZ transition that requires addition of an electron to the zero energy band while enhancing ZC transitions. On the other hand, removal of electrons activates the ZZ transitions, quenches ZC transitions and enhances VZ.

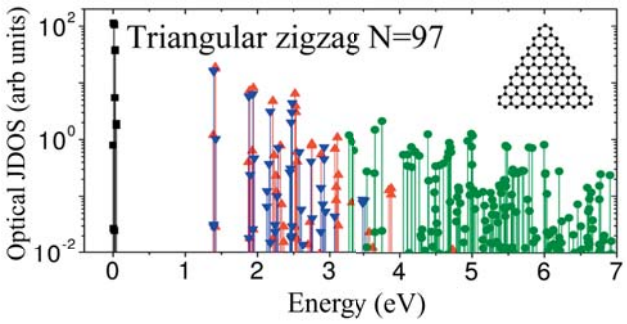

Figure 8 Joint density of states of a 97 atom triangular graphene quantum dot with zigzag edges. Black lines correspond to transitions within the zero energy band. Green lines are from valence to conduction band transition. Blue and red depicts valence-to-zero and zero-to-conduction band transitions, respectively. Reprinted from Ref. [18].

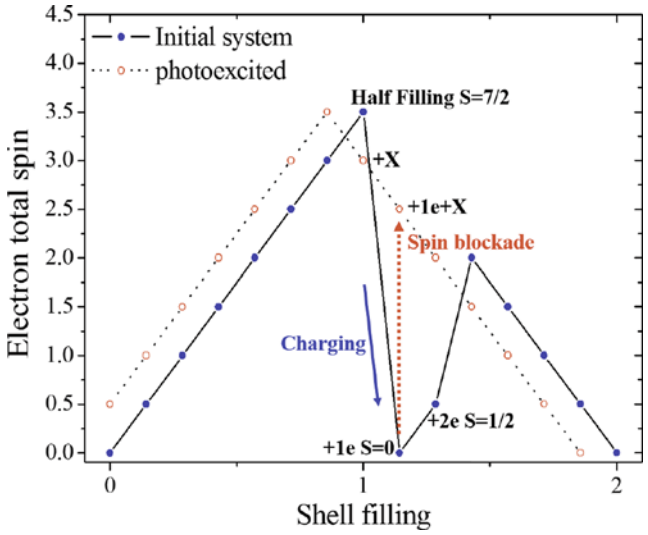

Figure 9 Electron total spin of the ground state as a function of zero-energy band filling. The solid and dashed lines compare the ground state without and with optical activation, respectively. The red dashed line depicts a disallowed transition due to spin blockade.

Especially in the TeraHertz regime, the transitions can be tuned by metallic gates. The ZZ transitions are turned off either at half filling, or by emptying/filling up the zero energy band. The total spin of the ground state becomes $S = 3$ upon removing an electron from the half filled band. The tHz transitions for such ground state correspond to the optically allowed excited states of a single hole. Addition of an electron to the total spin $S = 7/2$ ground state destroys the polarization of the band and the ground state becomes a highly correlated, $S = 0$ state. As a result, there are many allowed transitions from the $S = 0$ ground state leading to a very rich absorption spectrum. These variations in the optical spectra at the tHz regime are a good way of charge detection in graphene quantum dots.

In addition to altering the absorption spectrum, as discussed above, adding/removing an electron allows for manipulation of the magnetic moment of the ground state. As depicted in Fig. 9, adding an electron erases the magnetic moment, from $S = 7/2$ to $S = 0$. The magnetic moment can be restored by optical manipulation; exciting an electron from the valence band to the zero energy band, creates an exciton. The presence of the hole in the valence band restores the spin polarization of electrons in the zero energy band since the exchange energy between the hole and the zero-energy band electrons is maximal if the electron spins align. This results in an electron total spin $S_e = 5/2$ and a net spin (with the hole) $S = 3$ ground state.

10 Conclusion To summarize, we presented a theory of the optical properties of graphene quantum dots based on a combination of tight binding, Hartree–Fock and configuration interaction (CI) methods. The evolution of the band gap with lateral size and its renormalization by self-energy and excitonic effects was determined. For hexagonal and triangular graphene quantum dots a band of excitons, including bright degenerate singlet pair and a group of dark exciton states as well as a band of biexcitons was predicted. The exciton and biexciton spectrum was successfully compared with linear and transient absorption experiments on colloidal graphene quantum dots. Finally, the optical spin blockade in quantum dots with tunable carrier density and magnetic moments was described.

Acknowledgements I.O. and P.H. thank NSERC and A.D.G. acknowledges support from Bilim Akademisi – The Science Academy, Turkey, under the BAGEP program, and from Turkiye Bilimsel ve Teknolojik Arastirma Kurumu (TUBITAK), Turkey, under the BIDEP program.

References

[1] A. D. Guclu, P. Potasz, M. Korkusinski, and P. Hawrylak, Graphene Quantum Dots (Springer-Verlag, 2014).
[2] J. S. Bunch, Y. Yaish, M. Brink, K. Bolotin, and P. L. McEuen, Nano Lett. **5**, 287–290 (2005).
[3] L. A. Ponomarenko, F. Schedin, M. I. Katsnelson, R. Yang, E. W. Hill, K. S. Novoselov, and A. K. Geim, Science **320**, 356–358 (2008).
[4] B. Wunsch, T. Stauber, and F. Guinea, Phys. Rev. B **77**, 035316 (2008).
[5] J. Akola, H. P. Heiskanen, and M. Manninen, Phys. Rev. B **77**, 193410 (2008).
[6] T. Ihn, S. Gustavsson, U. Gasser, B. Küng, T. Muller, R. Schleser, M. Sigrist, I. Shorubalko, R. Leturcq, and K. Ensslin, Solid State Commun. **149**, 1419–1426 (2009).
[7] J. Wurm, A. Rycerz, I. Adagideli, M. Wimmer, K. Richter, and H. U. Baranger, Phys. Rev. Lett. **102**, 056806 (2009).
[8] F. Libisch, C. Stampfer, and J. Burgdörfer, Phys. Rev. B **79**, 115423 (2009).
[9] M. Ezawa, Phys. Rev. B **81**, 201402 (2010).
[10] P. Potasz, A. D. Guclu, and P. Hawrylak, Phys. Rev. B **81**, 033403 (2010).
[11] T. Yamamoto, T. Noguchi, and K. Watanabe, Phys. Rev. B **74**, 121409 (2006).
[12] J. Fernandez-Rossier and J. J. Palacios, Phys. Rev. Lett. **99**, 177204 (2007).
[13] M. Ezawa, Phys. Rev. B **76**, 245415 (2007).
[14] W. L. Wang, S. Meng, and E. Kaxiras, Nano Lett. **8**, 241–245 (2008).
[15] J. Jung and A. H. MacDonald, Phys. Rev. B **79**, 235433 (2009).
[16] L. C. Campos, V. R. Manfrinato, J. D. Sanchez-Yamagishi, J. Kong, and P. Jarillo-Herrero, Nano Lett. **9**, 2600–2604 (2009).
[17] A. D. Guclu, P. Potasz, O. Voznyy, M. Korkusinski, and P. Hawrylak, Phys. Rev. Lett. **103**, 246805 (2009).
[18] A. D. Guclu, P. Potasz, and P. Hawrylak, Phys. Rev. B **82**, 155445 (2010).
[19] M. L. Mueller, X. Yan, J. A. McGuire, and L. S. Li, Nano Lett. **10**, 2679–82 (2010).
[20] W. Sheng, M. Korkusinski, A. D. Guclu, M. Zielinski, P. Potasz, E. S. Kadantsev, O. Voznyy, and P. Hawrylak, Front. Phys. **7**, 328–352 (2012).

[21] J. Peng, W. Gao, B. K. Gupta, Z. Liu, R. Romero-Aburto, L. Ge, L. Song, L. B. Alemany, X. Zhan, G. Gao, S. A. Vithayathil, B. A. Kaipparettu, A. A. Marti, T. Hayashi, J. J. Zhu, and P. M. Ajayan, Nano Lett. **12**, 844–849 (2012).
[22] S. Kim, S. W. Hwang, M. K. Kim, D. Y. Shin, D. H. Shin, C. O. Kim, S. B. Yang, J. H. Park, E. Hwang, S. H. Choi, G. Ko, S. Sim, C. Sone, H. J. Choi, S. Bae, and B. H. Hong, ACS Nano **6**, 8203–8208 (2012).
[23] S. Kim, D. Hee Shin, C. Oh Kim, S. Seok Kang, S. Sin Joo, S. H. Choi, S. Won Hwang, and C. Sone, Appl. Phys. Lett. **102**, 053108 (2013).
[24] A. Guclu and P. Hawrylak, Phys. Rev. B **87**, 035425 (2013).
[25] X. Yan, B. Li, and L. S. Li, Acc. Chem. Res. **46**, 2254–2262 (2013).
[26] I. Ozfidan, M. Korkusinski, A. D. Guclu, J. A. McGuire, and P. Hawrylak, Phys. Rev. B **89**, 085310 (2014).
[27] I. Ozfidan, M. Korkusinski, and P. Hawrylak, Phys. Rev. B. **91**, 115314 (2015).
[28] C. Sun, F. Figge, I. Ozfidan, M. Korkusinski, X. Yan, L. shi Li, P. Hawrylak, and J. A. McGuire, Nano Lett. **15**, 5472–5476 (2015).
[29] W. Sheng, K. Luo, and A. Zhou, J. Chem. Phys. **142**, 021102 (2015).
[30] Y. Li, H. Shu, S. Wang, and J. Wang, J. Phys. Chem. C **119**, 4983–4989 (2015).
[31] C. Sun, F. Figge, J. A. McGuire, Q. Q. Li, and L. S. Li, Phys. Rev. Lett. **113**, 107401 (2014).
[32] S. Schumacher, Phys. Rev. B **83**, 081417 (2011).
[33] H. Riesen, C. Wiebeler, and S. Schumacher, J. Phys. Chem. A **118**, 5189 (2014).
[34] O. Benson, C. Santori, M. Pelton, and Y. Yamamoto, Phys. Rev. Lett. **84**, 2513 (2000).
[35] N. Akopian, N. Lindner, E. Poem, Y. Berlatzky, J. Avron, D. Gershoni, B. Gerardot, and P. Petroff, Phys. Rev. Lett. **96**, 130501 (2006).
[36] M. Shirane, Y. Igarashi, Y. Ota, M. Nomura, N. Kumagai, S. Ohkouchi, A. Kirihara, S. Ishida, S. Iwamoto, S. Yorozu, and Y. Arakawa, Physica E **42**, 2563–2566 (2010).
[37] M. Muller, S. Bounouar, K. D. Jons, M. Glassl, and P. Michler, Nature Photon. **8**, 224–228 (2014).
[38] J. Akola, H. P. Heiskanen, and M. Manninen, Phys. Rev. B **77**, 193410 (2008).
[39] Z. Z. Zhang, K. Chang, and F. M. Peeters, Phys. Rev. B **77**, 235411 (2008).
[40] P. Potasz, A. D. Guclu, and P. Hawrylak, Phys. Rev. B **82**, 075425 (2010).
[41] O. Voznyy, A. D. Guclu, P. Potasz, and P. Hawrylak, Phys. Rev. B **83**, 165417 (2011).
[42] P. Potasz, A. D. Guclu, O. Voznyy, J. A. Folk, and P. Hawrylak, Phys. Rev. B **83**, 174441 (2011).
[43] P. Potasz, A. D. Güçlü, A. Wójs, and P. Hawrylak, Phys. Rev. B **85**, 075431 (2012).
[44] M. Korkusinski, O. Voznyy, and P. Hawrylak, Phys. Rev. B **84**, 155327 (2011).
[45] A. D. Guclu, P. Potasz, and P. Hawrylak, Phys. Rev. B **88**, 155429 (2013).

